CONFERENCE PRE-PRINT

GLOBAL LINEAR DRIFT-WAVE EIGENMODE STRUCTURES ON FLUX SURFACES IN STELLARATORS: ION TEMPERATURE GRADIENT MODE

Hongxuan Zhu Princeton University Princeton, United States Email: hongxuan@princeton.edu

H. Chen and Z. Lin University of California, Irvine Irvine, United States

A. Bhattacharjee Princeton University Princeton, United States

Abstract

Turbulent transport greatly impacts the performance of stellarator magnetic confinement devices. While significant progress has been made on the numerical front, theoretical understanding of turbulence in stellarators is still lacking. In particular, due to nonaxisymmetry, different field lines couple within flux surfaces, the effects from which have yet to be adequately studied. The paper numerically simulate the linear electrostatic ion-temperature-gradient modes in stellarators using the global gyrokinetic particle-in-cell code GTC. It is found that the linear eigenmode structures are nonuniform across field lines on flux surfaces and are localized at the downstream direction of the ion diamagnetic drift. Based on a simple model from Zocco *et al.*, the paper shows that the localization can be explained from the nonzero imaginary part of the binormal wavenumber. It is further demonstrated that a localized surface-global eigenmode can be constructed from local gyrokinetic codes stella and GX, if one first solves the local dispersion relation with real wavenumbers at each field line, and then do an analytic continuation to the complex-wavenumber plane. These results suggest that the complex-wavenumber spectra from surface-global effects are required to understand the linear drift-wave eigenmode structures in stellarators.

1. INTRODUCTION

Turbulent transport significantly impacts the performance of stellarator magnetic confinement devices. For example, in the Wendelstein 7-X (W7-X) device, the ion-temperature-gradient (ITG) turbulence is believed to limit the achievable core ion temperature in electron-cyclotron-resonance-heated plasmas [1]. It is well known that plasma microturbulence is highly anisotropic in magnetic confinement devices, $l_{\parallel} \gg l_{\perp}$, where l_{\parallel} (l_{\perp}) is the characteristic wavelength along (across) the magnetic fields B. Therefore, fluctuating quantities such as the electrostatic potential Φ can be written as $\hat{\Phi}(\psi,\alpha,l)^{S(\psi,\alpha)/\rho_*}$, which consists of a rapidly varying phase factor e^{iS/ρ_*} and a slowly varying envelope $\hat{\Phi}$. Here, ψ is the flux-surface label, α is the field-line label, l is the distance along field lines, and $\rho_* = \rho_i/a$ is a small parameter with ρ_i the ion gyroradius at thermal velocity and a the minor radius of the device. Stellarators are nonaxisymmeric and the turbulent fluctuation level generally depends on both l and α . (We focus on the fluctuation level within flux surfaces, so that the dependence on ψ will not be discussed in this paper.) Such dependence could come from either the local effects, where the local geometric quantities vary with α , or the global effects, where fluctuations at different α couple together. To fully exploit the local effects, several flux tubes at different α , or a single flux tube with several poloidal turns, are often required for local simulations.

Despite the efforts in predicting turbulent transport from local simulations, there are open questions regarding the observed discrepancy between local and global simulation results on the turbulent fluctuation level in stellarators [2, 3]. For example, global gyrokinetic simulations found that the linear ITG eigenmodes are highly localized

in α , which is a common phenomenon in quasi-isodynamic (QI) W7-X configurations [4, 5], as well as in quasi-axisymmetric (QA) and quasi-helically symmetric (QH) configurations [6]. More recently, from global GENE-3D simulations of ITG turbulence in W7-X [4, 5], the fluctuation level noticeably deviates from stellarator symmetry, which local simulation results would always obey. Therefore, a careful study on the global effects is still needed.

In this work, we numerically simulate the linear electrostatic ITG eigenmodes in stellarators using the global gyrokinetic particle-in-cell code GTC, and present a theoretical explanation for the observed mode structures. We simulate the precise QA and the precise QH configurations reported in [7], as well as a W7-X high-mirror configuration used in [8]. We find that the linear eigenmode structures are nonuniform in α on flux surfaces and are localized at the downstream direction of the ion diamagnetic drift. Based on a simple model from Zocco [9, 10] and following the WKB theory of Dewar and Glasser [11], we show that the localization can be explained from the nonzero imaginary part of k_{α} . Focusing on the precise QA configuration, we further demonstrate that a localized surface-global eigenmode can be constructed from local gyrokinetic codes stella [12] and GX [13], if we first solve the local dispersion relation with real wavenumbers, and then do an analytic continuation to the complex-wavenumber plane. These results suggest that the complex-wavenumber spectra from surface-global effects are required to understand the linear drift-wave eigenmode structures in stellarators.

2. GTC SIMULATION OF GLOBAL LINEAR ITG EIGENMODE STRUCTURES

We use the global gyrokinetic particle-in-cell code GTC¹ to simulate linear electrostatic ITG eigenmodes in stellarators. The code utilizes Boozer coordinates (ψ,θ,ζ) , which are suitable for the nonaxisymmetric stellarator simulations. We simulate gyrokinetic deuterium ions with mass $m_i = 2m_p$ (m_p is the proton mass) and charge number $Z_i = 1$. Electrons are assumed adiabatic. Consistent with the convention in local simulations, we define the local density and temperature gradient scale lengths $L_n = (aB_a\partial_\psi \ln n_i)^{-1}$ and $L_T = (aB_a\partial_\psi \ln T_i)^{-1}$, and refer to a/L_n and a/L_T as the local gradients. Here, a is obtained from the quantity Aminor_p of the VMEC equilibria and $B_a = \psi_a/(\pi a^2)$, where ψ_a is the value of the toroidal magnetic flux ψ at the outermost flux surface. For our simulations we evaluate the ITG eigenmode structures in the region of constant temperature gradient a/L_T , while the density gradient is set to be zero, $a/L_n = 0$. In our simulations, we use 2000 grids in the poloidal direction (about 40 grids per wave period), 40 radial grids in the domain 0.35 < r/a < 0.65, and require the electrostatic potential $\delta\Phi$ to vanish at the radial boundaries. We simulate 15 toroidal planes spanning one field period of the devices. Approximately 100 ions are simulated for each grid point in the 3D domain, and the simulation time step size is $t = 0.01R_0/v_{\rm ti}$ with R_0 the toroidally averaged major radius of the magnetic axis.

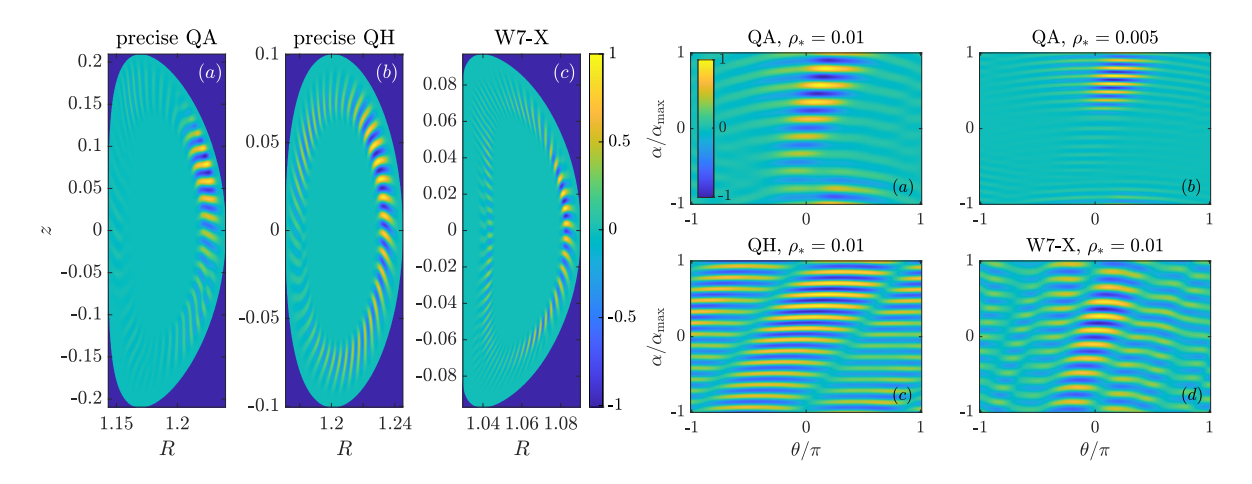


FIG. 1. Left: the linear global ITG eigenmode structures in cylindrical coordinates (R, z) at toroidal Boozer angle $\zeta = 0$. Right: the same eigenmode structures in the field-line following coordinates (α, θ) .

The ITG eigenmode structures at toroidal $\zeta=0$ are plotted in figure 1. The modes rotate counter-clockwise in the direction of ion diamagnetic drift, while their amplitudes increase exponentially in time. Due to stellarator symmetry, the configurations are up-down symmetric at $\zeta=0$. However, the mode structures are up-down asymmetric, and are localized at the upper part of the plane, which is the downstream direction of the ion diamagnetic drift. Also shown in figure 1 are the mode structures in the field-line following coordinates (α,θ) on the r/a=0.5 flux surface, where $\alpha=\theta-\iota\zeta$ is the field-line label, ι is the rotational transform, and we use the poloidal angle θ instead of the distance along field lines l as the parallel coordinate. It is seen that the mode structures do not

¹https://sun.ps.uci.edu/gtc

obey stellarator symmetry, which states that geometric quantities are the same at (α, θ) and $(-\alpha, -\theta)$. Instead, the modes are localized at $\alpha > 0$, which results in the up-down asymmetry. We also found that the localization becomes more pronounced at smaller ρ_* , as seen from the mode structures in the QA at a smaller ρ_* . This behavior will be explained below, where we conclude that the localization increases exponentially with ρ_*^{-1} .

3. THEORETICAL EXPLANATION FROM A SIMPLE MODEL

Zocco *et al.* proposed a simple model to study the mode structures across field lines [9, 10]. The model considers the limit of large temperature gradient, $a/L_T\gg 1$, so that the ITG mode is concentrated at the bad-curvature region along field lines and the θ -dependence of the mode structure is not considered. Then, the model becomes a 1D differential equation in α which describes the global eigenmode structures as well as their frequencies. Letting $y=\alpha/\iota$ so that $y\in [-\pi,\pi]$, the mode structure $\Phi(y)$ is described from

$$\left(\omega^2 - \rho_*^3 g \omega \partial_y^3 - \rho_*^2 f \partial_y^2\right) \Phi(y) = 0. \tag{1}$$

Here, ω is the eigenmode frequency, and g(y) and f(y) are functions of y that model the field-line dependent stellarator geometry. An example of the solution is shown in figure 2 with $\rho_*=0.05, f=1, g=1-0.2\cos y$, and the most unstable global eigenmode corresponds to $\omega=0.66+0.89i$. The mode is localized around $y=\pi/2$, consistent with the GTC results of mode localization at $\alpha>0$. Zocco obtained a similar localized solution with a different set of parameters more relevant to W7-X, again suggesting that the localization is a universal feature, but a comprehensive understanding of this feature is still missing.

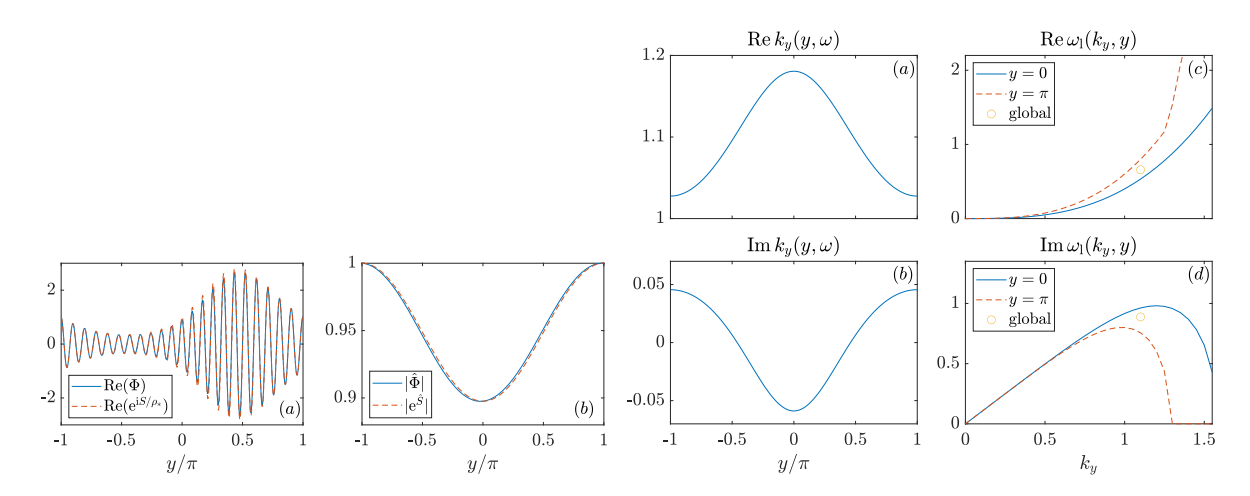


FIG. 2. Left: comparison of numerical and analytical solution of equation (1). Right (a) and (b): the real and imaginary part of the global solution of k_y . Right (c) and (d): the local frequency and growth rates versus real k_y at two different flux tubes y=0 and $y=\pi$, as well as the global eigenmode frequency and growth rate.

In the following, we study the mode structure from a WKB analysis similar to Dewar and Glasser [11]. Since $\Phi(y) = \hat{\Phi}(y)e^{iS(y)/\rho_*}$, we replace ∂_y with $i\partial_y S/\rho_* + \partial_y$, where ∂_y no longer acts on the phase factor. To the lowest order in ρ_* , equation (1) becomes

$$\omega^2 - gk_y^3\omega + fk_y^2 = 0, \quad k_y(y) = \partial_y S,$$
(2)

which gives the local dispersion relation $\omega = \omega_l(k_y, y)$. To the next order in ρ_* , we obtain an equation for the envelope $\hat{\Phi}$:

$$\frac{\partial_y \hat{\Phi}}{\hat{\Phi}} = -\frac{\partial_y k_y}{k_y} \frac{3gk_y \omega - f}{3gk_y \omega - 2f}.$$
 (3)

Therefore, the global solution is $\Phi=e^{\hat{S}}e^{iS/\rho_*}$ with

$$S(y) = \int_0^y k_y(s)ds, \quad \hat{S}(y) = -\int_0^y \frac{\partial_s k_y(s)}{k_y(s)} \frac{3g(s)k_y(s)\omega - f(s)}{3g(s)k_y(s)\omega - 2f(s)}ds. \tag{4}$$

As shown in figure 2, the numerical solution of Φ is well approximated by the phase factor e^{iS/ρ_*} . The numerically calculated envelope $\hat{\Phi}$ also agrees well with the next-order result $e^{\hat{S}}$. However, the variation in $|\hat{\Phi}|$ is insignificant

compared to the exponentially varying phase factor, and hence we conclude that the mode localization mainly comes from the phase factor e^{iS/ρ_*} .

To understand the localization at y>0, we solve for S from equations (2) and (4). Since ω is constant while f and g vary in y (though f is constant for the example shown here), k_y must vary with y too. Namely, we solve for $k_y(y,\omega)$ at given ω . The solution is shown in figure 2. The imaginary part of k_y is nonzero, $\operatorname{Im} k_y \approx -0.05 \cos y$. Consequently, the phase factor has a nonuniform amplitude,

$$|e^{iS/\rho_*}| \approx e^{(0.05\sin y)/\rho_*},\tag{5}$$

which is localized around $y = \pi/2$. Therefore, the localization is due to the negative $\operatorname{Im} k_y$ at y = 0 and increases exponentially with ρ_*^{-1} . The imaginary part of k_y can be intuitively understood by approximately solving k_y from the first-order Taylor expansion:

$$k_y \approx k_{y0} + \left(\frac{\partial \omega_l}{\partial k_y}\right)^{-1} \Delta \omega, \quad \Delta \omega = \omega - \omega_l.$$
 (6)

Since we are looking at the most unstable eigenmode where $\partial(\operatorname{Im}\omega)/\partial k_y\approx 0$, the sign of $[\partial(\operatorname{Re}\omega)/\partial k_y]^{-1}\operatorname{Im}\Delta\omega$. Therefore, we identify two reasons that lead to the negative $\operatorname{Im}k_y$ at y=0: (i) the global eigenmode growth rate is smaller than the local growth rate at y=0, $\operatorname{Im}\Delta\omega<0$ (figure 2); and (ii) the ion diamagnetic drift is defined to be in the positive-y direction, so that $\partial(\operatorname{Re}\omega)/\partial k_y>0$. In other words, if the y=0 flux tube gives the largest local ITG growth rate, then the localization of the ITG modes will occur at the downstream side of the ion diamagnetic drift.

4. CONSTRUCTION OF A SURFACE-GLOBAL SOLUTION FROM LOCAL GYROKINETIC SIMULATION RESULTS

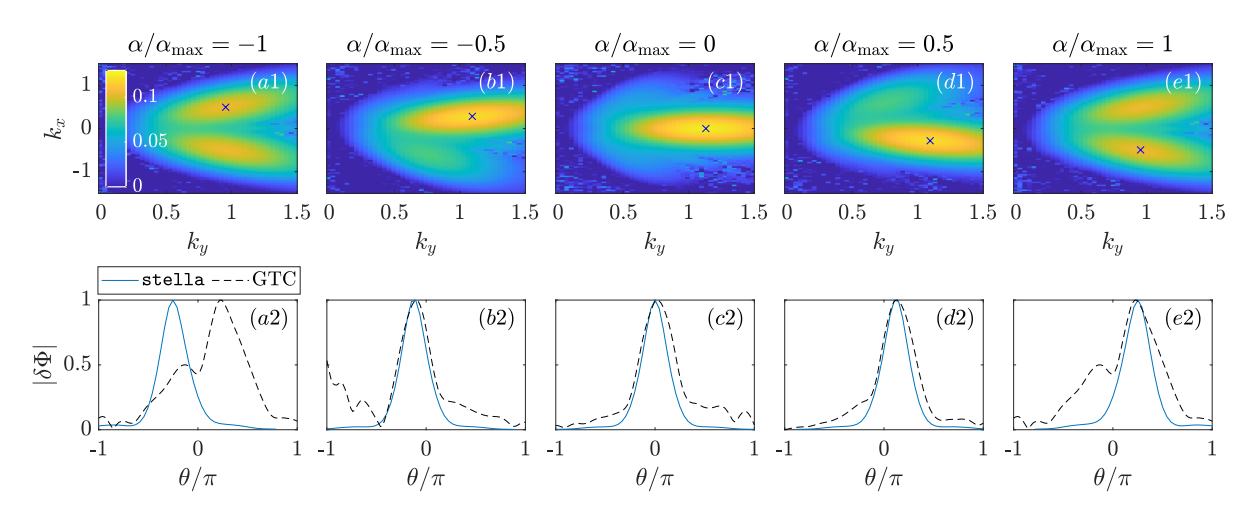


FIG. 3. Comparison between results from local stella simulations and global GTC simulations. First row: the local growth rates $\operatorname{Im} \omega_l$ versus (k_x, k_y) at different α . The blue crosses indicate the most unstable local solution. Second row: the eigenmode amplitudes $|\delta\Phi|$ versus θ , which are normalized to their maxima at each α .

Based on the results from above, we construct a surface-global solution from local gyrokinetic simulations, and compare the results with the GTC solution. In particular, we focus on the precise QA configuration here. First, we obtain the local dispersion relation $\omega = \omega_l(\boldsymbol{k},\alpha)$ with real $\boldsymbol{k} = k_r \nabla r + k_\alpha \nabla \alpha$. Then, we calculate the complex \boldsymbol{k} from first-order Taylor expansion, and construct a surface-global solution using the complex \boldsymbol{k} . Finally, we compare the constructed solutions with the GTC solutions.

We use local gyrokinetic codes stella [12] and GX [13] to obtain $\omega_l(k,\alpha)$ at the r/a=0.5 flux surface. For each field line α , we choose the flux tube to span one poloidal turn, $\theta \in [-\pi, \pi]$, so that different flux tubes are simulated independently. After obtaining the local dispersion relation with real k, we look for complex $k(\alpha)$ such that $\omega_l(k(\alpha), \alpha) = \omega$ is constant. Similar to the previous section, this is done from first-order Taylor expansion:

$$\mathbf{k}(\alpha) \approx \mathbf{k}_0(\alpha) + \left(\frac{\partial \omega_l}{\partial k}\right)^{-1} \Delta \omega, \quad \Delta \omega = \omega - \omega_l.$$
 (7)

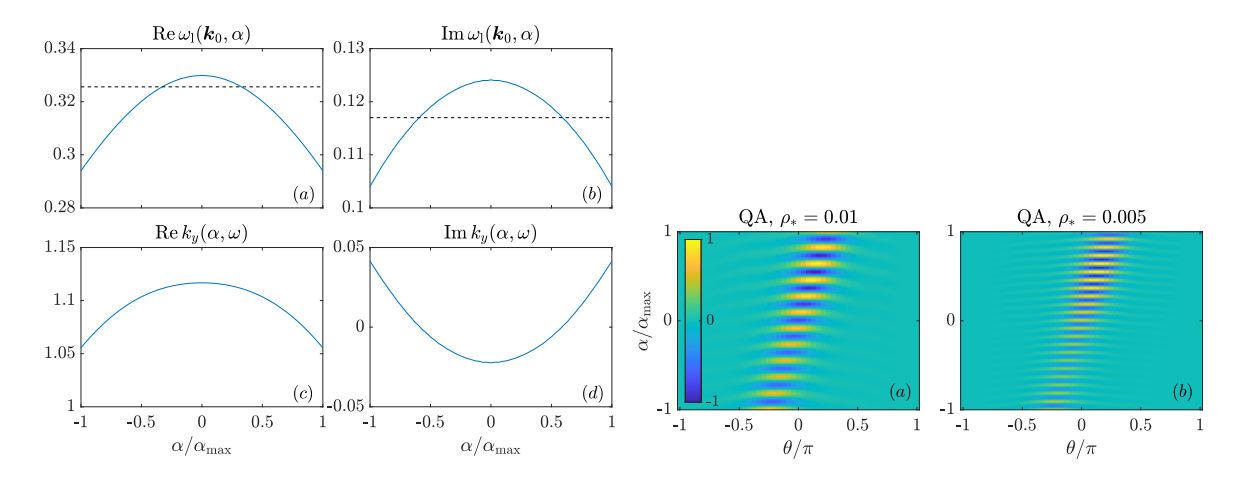


FIG. 4. Left (a) and (b): the real and imaginary parts of ω versus α at $\mathbf{k} = \mathbf{k}_0$ from stella (blue solid curves) and the calculated surface-global eigenmode frequency ω (black dashed line). Left (c) and (d): solution of k_y from first-order Taylor expansion (7). Right (a) and (b): The constructed surface-global solution (9) from local stella solutions with (a) $\rho_* = 0.01$ and (b) $\rho_* = 0.005$.

Here, $\mathbf{k}_0 = (k_{x0}, k_{y0})$ is real, ω is the surface-global eigenmode frequency to be determined in the following, and ω_l and $\partial_{\mathbf{k}}\omega_l$ are evaluated at $\mathbf{k} = \mathbf{k}_0$. The exact value of \mathbf{k}_0 is not important as long as it is close to \mathbf{k} so that equation (7) is valid. Note that both \mathbf{k} and $\partial_{\mathbf{k}}\omega_l$ are 2D vectors and numerically we look for $\Delta\mathbf{k} = \mathbf{k} - \mathbf{k}_0$ that minimizes $|\Delta\mathbf{k} \cdot \partial_{\mathbf{k}}\omega - \Delta\omega|$. In other words, although local simulations only provide the information on the real- \mathbf{k} plane, we can still obtain the information on the complex- \mathbf{k} plane from analytic continuation.

The local growth rates $\operatorname{Im} \omega_l$ versus (k_x,k_y) from stella are plotted in the first row of figure 3, which shows that the fastest growing modes correspond to nonzero k_x . The most unstable modes are marked by the blue crosses in the figure, and are approximately given by

$$k_{x0} = -0.5\alpha/\alpha_{\text{max}}, \quad k_{y0} = 1.13 - 0.175(\alpha/\alpha_{\text{max}})^2.$$
 (8)

The mode amplitudes $|\delta\Phi(\theta)|$ at k_0 are shown in the second row of figure 3, where we also plot the GTC results. Due to stellarator symmetry, the local results are symmetric with respect to the coordinate change $(\alpha,\theta,k_x)\to (-\alpha,-\theta,-k_x)$. As shown in the figure, the local eigenmode structures qualitatively resemble the GTC results. Note that the GTC solution is periodic in α , but the local solution (8) is not, which transitions from $k_{x0}=0.5$ at $\alpha/\alpha_{\max}=-1$ to $k_{x0}=-0.5$ at $\alpha/\alpha_{\max}=1$. In fact, the GTC solution of $|\delta\Phi|$ has two peaks at $\alpha/\alpha_{\max}=\pm 1$, which appears to be a superposition of the two local solutions at $k_{x0}=\pm 0.5$. Therefore, the local solution lives on an extended α space, $\alpha\in(-\infty,\infty)$, and the periodicity of the global solution can be recovered from a superposition of the local solutions.

The local eigenmode real frequencies and growth rates at $k = k_0$ are plotted in figure 4. To determine the surface-global eigenmode frequency ω , we assume that the corresponding solution k from (7) satisfies $\int d\alpha \operatorname{Im} k_y = 0$. The corresponding solutions for k_y are also shown in the figure. In particular, $\operatorname{Im} k_y$ is nonzero and is negative at $\alpha = 0$, which leads to the localization at $\alpha > 0$.

Finally, with the complex k, we construct a surface-global solution as

$$\delta\Phi_{\text{global}}(\theta,\alpha) = \delta\Phi_{\text{local}}(\theta;\alpha,k_0)e^{iS(\alpha)/\rho_*}, S = \int d\alpha \, k_y(\alpha)r/a, \tag{9}$$

where $\delta\Phi_{\rm local}$ is the normalized local eigenmode structure from stella at $k=k_0$ for each α . The results are shown in figure 4 with $\rho_*=0.01$ and $\rho_*=0.005$, which are not periodic in α because we only consider one period in α for the local solution. Nevertheless, the constructed solutions look similar to the GTC results in figure 1. The increasing level of localization with decreasing ρ_* is also reproduced as a direct consequence from the phase factor in equation (9). We conclude that for the linear ITG mode structures in the stellarator configurations, many features of the global GTC solution can be reproduced from the constructed surface-global solution, if we first solve the local dispersion relation with real k, and then do an analytic continuation to the complex k.

5. CONCLUSIONS AND DISCUSSIONS

We numerically simulate the linear electrostatic ITG eigenmodes in stellarators using the global gyrokinetic particle-in-cell code GTC, and present a theoretical explanation for the observed mode structures. We find that the

linear eigenmode structures are localized at the downstream direction of the ion diamagnetic drift. Based on a simple model from Zocco $et\ al.\ [9,10]$ and following the WKB theory of Dewar and Glasser [11], we show that the localization can be explained from the nonzero imaginary part of k_{α} . Focusing on the precise QA configuration, we further demonstrate that a localized surface-global eigenmode can be constructed from local gyrokinetic codes stella and GX, if we first solve the local dispersion relation with real wavenumbers, and then do an analytic continuation to the complex-wavenumber plane. These results suggest that the complex-wavenumber spectra from surface-global effects are required to understand the linear drift-wave eigenmode structures in stellarators.

While the conclusions in this work are limited to the linear instabilities, they could be useful in interpreting nonlinear simulation results. For example, the nonlinear fluctuation level of ITG turbulence in W7-X deviates from stellarator symmetry [4, 5] and its localization is consistent with (although not as pronounced as) the linear results. The linear and nonlinear thresholds for the ITG turbulence in a QA stellarator appears to lie above that of the most unstable flux tube [14], which is also consistent with the conclusion that the global eigenmode growth rate is below the most unstable flux tube. Quantitative studies of these effects, including whether the observed surface-global effects can reduce the gap between local and global predictions on the turbulent transport, will be the subject of future work.

ACKNOWLEDGEMENTS

H.Z. thanks R. Gaur for providing scripts that calculate flux-tube quantities from VMEC equilibrium. H.Z. was supported by a grant from the Simons Foundation/SFARI (Grant #560651, AB). This research used resources of the National Energy Research Scientific Computing Center, which is supported by the Office of Science of the U.S. Department of Energy under Contract No. DE-AC02-05CH11231.

REFERENCES

- [1] Beurskens M, Bozhenkov S A, Ford O, Xanthopoulos P, Zocco A, Turkin Y, Alonso A, Beidler C, Calvo I, Carralero D et al. 2021 Nuclear Fusion **61** 116072.
- [2] Xanthopoulos P, Mynick H, Helander P, Turkin Y, Plunk G, Jenko F, Görler T, Told D, Bird T and Proll J 2014 Physical Review Letters **113** 155001.
- [3] Wilms F, Navarro A B and Jenko F 2023 Nuclear Fusion 63, 086004.
- [4] Bañón Navarro A, Merlo G, Plunk G, Xanthopoulos P, Von Stechow A, Di Siena A, Maurer M, Hindenlang F, Wilms F and Jenko F 2020 Plasma Physics and Controlled Fusion **62** 105005.
- [5] Sánchez E, Bañón Navarro A, Wilms F, Borchardt M, Kleiber R and Jenko F 2023 Nuclear Fusion **63** 046013.
- [6] Chen H, Wei X, Zhu H and Lin Z 2025 Nuclear Fusion 65 074002.
- [7] Landreman M and Paul E 2022 Physical Review Letters 128 035001.
- [8] Gonzále-Jerez A, Xanthopoulos P, García-Regaña J, Calvo I, Alcusón J, Bañón Navarro A, Barnes M, Parra F and Geiger J 2022 Journal of Plasma Physics 88 905880310
- [9] Zocco A, Plunk G, Xanthopoulos P and Helander P 2016 Physics of Plasmas 23, 082516.
- [10] Zocco A, Plunk G and Xanthopoulos P 2020 Physics of Plasmas 27, 022507.
- [11] Dewar R and Glasser A 1983 The Physics of Fluids 26 3038.
- [12] Barnes M, Parra F I and Landreman M 2019 Journal of Computational Physics 391 365.
- [13] Mandell N R, Dorland W, Abel I, Gaur R, Kim P, Martin M and Qian T 2024 Journal of Plasma Physics **90** 905900402.
- [14] Xanthopoulos P, Plunk G, Zocco A and Helander P 2016 Physical Review X 6 021033.